Mon. Not. R. Astron. Soc. **000**, 000–000 (0000) Printed 17 June 2014 (MN LATEX style file v2.2)

On the spine-layer scenario for the very high-energy emission of NGC 1275

F. Tavecchio[1⋆] and G. Ghisellini[1]
[1]*INAF – Osservatorio Astronomico di Brera, via E. Bianchi 46, I–23807 Merate, Italy*

arXiv:1404.6894v2 [astro-ph.HE] 16 Jun 2014

17 June 2014

ABSTRACT
We discuss the γ–ray emission of the radiogalaxy NGC 1275 (the central galaxy of the Perseus Cluster), detected by *Fermi*–LAT and MAGIC, in the framework of the "spine-layer" scenario, in which the jet is assumed to be characterized by a velocity structure, with a fast spine surrounded by a slower layer. The existence of such a structure in the parsec scale jet of NGC 1275 has been recently proved through VLBI observations. We discuss the constraints that the observed spectral energy distribution imposes to the parameters and we present three alternative models, corresponding to three different choices of the angles between the jet and the line of sight ($\theta_{\rm v} = 6^\circ, 18^\circ$ and 25°). While for the the case with $\theta_{\rm v} = 6^\circ$ we obtain an excellent fit, we consider this solution unlikely, since such small angles seems to be excluded by radio observations of the large-scale jet. For $\theta_{\rm v} = 25^\circ$ the required large intrinsic luminosity of the soft (IR–optical) component of the spine determines a large optical depth for γ–rays through the pair production scattering $\gamma\gamma \rightarrow e^+e^-$, implying a narrow cut–off at ~ 50 GeV. We conclude that intermediate angles are required. In this case the low frequency and the high–energy emissions are produced by two separate regions and, in principle, a full variety of correlations is expected. The correlation observed between the optical and the γ–ray flux, close to linearity, is likely linked to variations of the emissivity of the spine.

Key words: radiation mechanisms: non-thermal — γ–rays: general —γ–rays: galaxies

1 INTRODUCTION

The extragalactic sky at very–high energies (VHE; $E > 50$ GeV) is dominated by blazars, radio–loud active galactic nuclei with relativistic jets pointing toward the Earth. This geometry is particularly favorable since, due to the relativistic aberration, the resulting non–thermal emission of the jet is strongly amplified and blue shifted. The spectral energy distribution (SED) of blazars displays two broad components, the one peaking in the IR–UV band produced by relativistic electrons through synchrotron emission, and the high–energy one (peaking in γ–rays) attributed, in the so–called one–zone leptonic models, to the inverse Compton (IC) emission by the same electrons (e.g., Ghisellini et al. 1998). The parameter regulating the amplification of the emitted radiation, the relativistic Doppler factor $\delta \equiv [\Gamma(1-\beta\cos\theta_{\rm v})]^{-1}$ (where Γ is the bulk Lorentz factor of the flow and $\beta = v/c$), is strongly dependent on the angle between the jet axis and the line of sight, $\theta_{\rm v}$: it is maximal within a cone with semi–aperture $\theta_{\rm v} \simeq 1/\Gamma$ and drops rapidly outside it. In this scheme thus one expects that for viewing angles larger than $1/\Gamma$ the jet non–thermal luminosity becomes increasingly fainter. Accordingly to this expectation, only a handful of radiogalaxies – thought to be the *parent* (i.e. not beamed at us) population of blazars – have been detected in VHE γ–rays (Aharonian et al. 2006, 2009, Aleksic et al. 2012).

In the simple scheme sketched above, the SED of radiogalaxies should resemble that of blazars, the only difference being the reduced beaming. However, as discussed in e.g., Tavecchio & Ghisellini (2008, TG08 hereafter) and Aleksic et al. (2014, A14 hereafter), the relatively large separation of the frequencies of two peaks, coupled to the expected low Doppler factor ($\delta \simeq 2-4$) is difficult to reproduce with one–zone emission models. Indeed, there are indications that the jet structure is not as simple as that assumed above. There is compelling observational evidence that the jet of low–power TeV blazars could be structured (e.g. Giroletti 2008), with a fast (with bulk Lorentz factor $\Gamma_{\rm s} = 10-20$) central spine, surrounded by a slower ($\Gamma_{\rm l} = 2-4$) layer. A structure of this type is also required to unify BL Lacs objects with the parent population of FRI radiogalaxies (Chiaberge et al. 2000). From the point of view of the radiative properties, such a structure leads to the enhancement of the radiative efficiency of both components, since the electrons of each region can inverse–Compton scatter the beamed soft photons coming from the other (Ghisellini et al. 2005). As shown in Ghisellini et al. (2005) this model can account for the VHE emission of TeV detected blazars (thought to be produced in the spine) and predicts that the weakly beamed emission of the layer could dominate the emission from misaligned radiogalaxies.

⋆ E–mail: fabrizio.tavecchio@brera.inaf.it

© 0000 RAS

This scheme was successfully applied to the modeling of the SED of the first radiogalaxy detected at VHE, M87 (TG08). The same idea is at the base of the decelerating jet scenario, in which one assumes that the inner jet moves faster then the outer jet zones. Also in this scenario the faster and the slower regions can interact through their radiation fields (Georganopoulos & Kazanas 2003).

NGC 1275, located in the Perseus cluster ($D \simeq 75$ Mpc) is one of the closest radiogalaxies. It has been the subject of intense study in the last years, particularly in view of the evident impact of the relativistic jets on the gas of the surrounding cluster (e.g. Fabian et al. 2011). At high energy it was not detected by EGRET onboard *CGRO* flown in the nineties. Instead, *Fermi*–LAT detected NGC 1275 soon after its launch (Abdo et al. 2009), with a flux 4 times larger than the EGRET upper limit, implying secular variability of the high-energy flux. The γ–ray emission is variable also on much smaller timescales, down to a week (Kataoka et al. 2010, Brown & Adams 2011). Radio observations revealed an increasing of the activity starting in 2005 (Abdo et al. 2009) and recent VLBI observations (Nagai et al. 2010, 2014) show a new radio component ejected from the core. NGC 1275 has been the third radiogalaxy detected in the VHE band (by MAGIC), showing a very soft spectrum smoothly connected to the GeV spectrum (Aleksic et al. 2012). A14 report multifrequency data obtained during two multifrequency campaigns held in 2010–2011, thanks to which the overall SED could be assembled. Unfortunately, the available X-ray spectrum, probing the critical region of the SED between the two bumps, is affected by strong pile-up and it was not possible to fix the slope of the underlying non–thermal power law. The SED is barely compatible with a one-zone leptonic model for the values of the viewing angle usually considered in literature.

The problem with the one–zone model is that, with the small Doppler factors corresponding to the large $\theta_{\rm v}$, it is difficult to reproduce the required large separation of the frequencies of the two peaks. Similar to the case of M87, it is tempting to think that a solution is to admit a structured jet. In fact, strong observational support to this scenario is provided by the clear evidence for a spine–sheath structure shown in recent VLBA maps presented in Nagai et al. (2014). The observed limb–brightened structure suggests the presence of a faster central core and a slower sheath for the inner (i.e. parsec scale) jet. For an assumed angle of $25^{\rm o}$ and with the hypothesis of equal rest-frame emissivity, the data are consistent with a bulk Lorentz flow of the sheath of 2.4. Motivated by this observational evidence and by the difficulties of the one-zone model, in the following we will explore the applicability of the spine–layer scenario of Ghisellini et al. (2005) to the multifrequency emission of NGC 1275.

After a discussion of the SED (§2) we will describe the model and its application (§3). We discuss the results in §4. Throughout the paper, we assume the following cosmological parameters: $H_0 = 70$ km s^{-1} Mpc^{-1}, $\Omega_{\rm M} = 0.3$, $\Omega_\Lambda = 0.7$.

2 THE SPECTRAL ENERGY DISTRIBUTION

The SED of NGC 1275 during the first MAGIC campaign (A14) is reported in Fig. 1. Red symbols show almost simultaneous data, green lines are for historical data (see A14 for references). Although the covering of the low–frequency region is relatively sparse, one can identify two components, one traced by the radio and optical data, the other one well tracked by *Fermi*–LAT and MAGIC data points. The gray line shows a power law spectrum of the central emission from NGC 1275 derived from *Chandra* observations. As discussed in A14, the observation is affected by a strong pile–up. This, coupled with the complexity of the emission from the central regions of NGC 1275 (which includes several contributions, mainly the thermal emission of the cluster and host galaxy gas), makes impossible to determine a unique fit. A14 report different fits of the X-ray spectrum, corresponding to different fixed values of the spectral index of the power law. Considering the goodness of the fit, the best solution would correspond to a relatively flat spectrum, with photon index 1.7. Other possible solutions, however, include steeper spectra. In particular A14 adopt the solution corresponding the a photon index of 2.5 (dashed gray line in the top panel of Fig. 1), which is compatible with the slope of the high–energy tail of the synchrotron component of the one–zone model. Although possible, this slope is however rather different than that previously derived for the soft and hard X–ray spectra (green bow–ties, Balmaverde et al. 2006, Ajello et al. 2009), which consistently trace a power law continuum with slope ≈ 1.7. However, the flux corresponding to the latter slope (solid gray line in the left panel) is exceptionally high, not compatible with the optical datapoint and the LAT spectrum. Given these large uncertainties we choose to use the historical X-ray data (green) for our modeling. With this choice the low–energy components of the SED has to peak between the radio and the optical band, with the optical associated to the high–energy tail of the component. This is different from the model discussed in A14, for which the synchrotron component was instead located in the UV band, with the optical and the (steep) X–ray emission associated to the low and high frequency tails of the synchrotron emission.

3 MODELLING

3.1 One–zone synchrotron-self Compton model

As discussed A14, the modeling of the SED within the one-zone SSC scenario is challenging. A14 performed their analysis in the case of a large synchrotron frequency (in the soft X-ray band); their arguments are even more compelling in our interpretation, with the SED peak below the optical band. In fact, as detailed by TG08 for the case of M87, the main problem is represented by the large separation between the two SED peaks, which unavoidably implies huge Doppler factors, incompatible with the large viewing angle inferred for radiogalaxies. Adapting the limit obtained in TG08 for the numerical values suitable for NGC 1275, the SED constrains the Doppler factor to be larger than:

$$\delta \simeq 450\, L_{\rm s,43.5}^{1/2}\, L_{\rm IC,43.3}^{-1/4}\, \nu_{\rm s,13}^{-1}\, \nu_{\rm IC,24}^{1/2} t_{\rm var,1\ w}^{-1/2}, \qquad (1)$$

where $L_{\rm s}$ and $L_{\rm IC}$ are the synchrotron and IC luminosities, $\nu_{\rm s}$ and $\nu_{\rm IC}$ the synchrotron and IC peak frequencies and we assume a (conservative) variability timescale $t_{\rm var} = 1$ week.

We therefore exclude the one-zone SSC model and in the following we discuss the structured jet scenario.

3.2 The structured jet scenario

We briefly recall the main features and the parameters of the model fully described in Ghisellini et al. (2005) and TG08. The spine is assumed to be a cylinder with eighth H_s and radius R_s. The subscripts "s" and "l" stand for spine and layer, respectively. The layer is a hollow cylinder with height H_l, internal radius R_s and external radius $R_l = 1.2 \times R_s$. As for the case of M87, we assume that $H_s \ll H_l$, corresponding to the case of a perturbation (e.g.

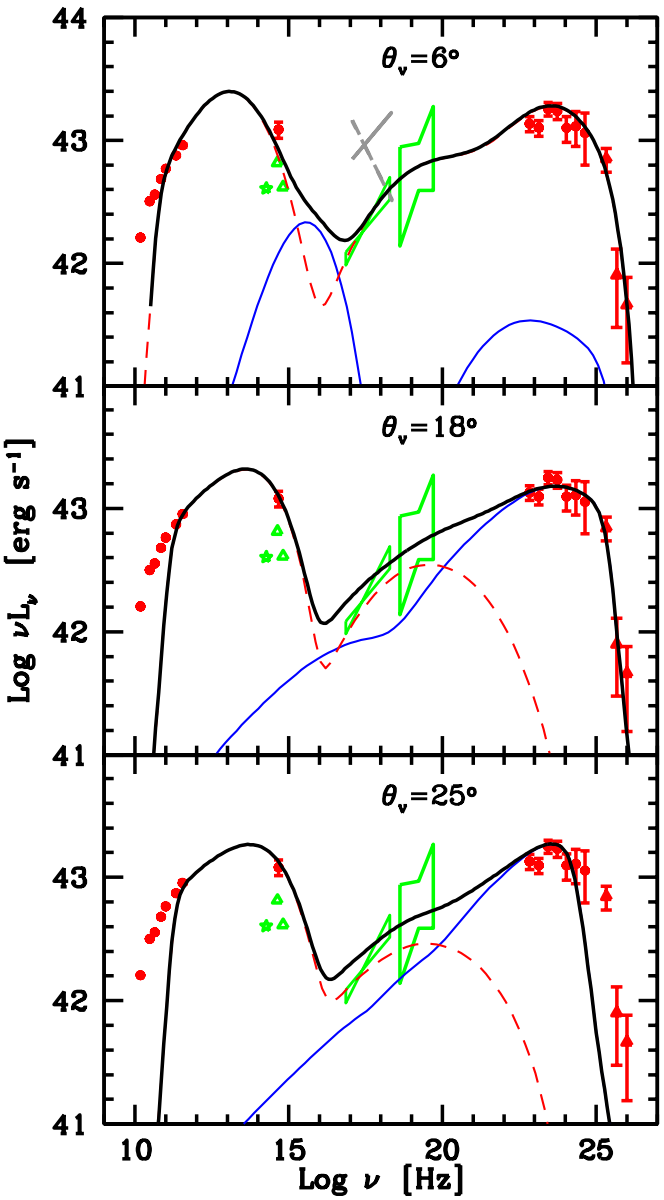

Figure 1. Spectral energy distribution of the core of NGC 1275 during the first MAGIC campaign reported in Aleksic et al. (2014). Red symbols show the quasi simultaneous multifrequency data. The green points in the optical band are historical data from Chiaberge et al. (1999) and Baldi et al. (2010). Green "bow-ties" in the X–ray band are from Balmaverde et al. (2006) and Ajello et al. (2009). The dashed (solid) gray line in the top panel shows the *Chandra* spectrum assuming a photon index of 2.5 (1.7). We refer to Aleksic et al. (2014) for details. The three panels report the results of our structured jet emission model for two different values of the viewing angle, from top to bottom: $\theta_{\rm v} = 6^{\rm o}$, $\theta_{\rm v} = 18^{\rm o}$ and $\theta_{\rm v} = 25^{\rm o}$. The red (dashed) and the blue (solid) lines show the emission from the spine and the layer, respectively. The thick black line shows the total. See text for details.

a shock) traveling down the the spine, surrounded by a relatively long and stationary layer of slow plasma, possibly resulting from the interaction of the edge of the jet with the external medium.

Electrons in both zones follow a broken power law energy distribution, specified by the minimum, the maximum and the break Lorentz factors $\gamma_{\rm min}$, $\gamma_{\rm max}$ and $\gamma_{\rm b}$ and indices n_1 and n_2. The model assumes that the electron energy distribution is stationary and it does not take into account the electron radiative losses. The normalization of the electron distribution is parametrized by the emitted synchrotron luminosity, $L_{\rm syn}$. The emitting regions are filled with a tangled magnetic field B_s, B_l. The relativistic beaming is specified by the two Lorentz factors Γ_s, Γ_l and by the viewing angle $\theta_{\rm v}$.

Electrons emit synchrotron and IC radiation. For the latter, besides the local synchrotron radiation field (SSC emission) we also consider the radiation field of the other component. Due to the relative motion, the energy density of the radiation field of one component in the rest frame of the other is boosted by the squared of the relative Lorentz factor, $\Gamma_{\rm rel} = \Gamma_{\rm s}\Gamma_{\rm l}(1-\beta_{\rm s}\beta_{\rm l})$. In the calculations we also take into account the absorption of γ–rays through the interaction with the soft radiation field, $\gamma\gamma \rightarrow e^+e^-$. Since the radiation is produced and absorbed within the same region, the "suppression factor" due to absorption is $I(\nu)/I_{\rm o}(\nu) = \{1-\exp[-\tau_{\gamma\gamma}(\nu)]\}/\tau_{\gamma\gamma}(\nu)$ which, for large optical depths, simply becomes $1/\tau_{\gamma\gamma}$.

For a fixed viewing angle $\theta_{\rm v}$, the (bolometric) synchrotron and SSC luminosities of both components are amplified by the usual boosting factors $\delta_{\rm s}^4$ and $\delta_{\rm l}^4$. The IC emission from the scattering of the radiation field produced in the other component follows a more complex pattern, involving the relative Doppler factors between the two components (see TG08 for a detailed discussion).

Although the number of the parameters is large (almost twice that of the simple SSC model), the model has to satisfy other constraints that can be used as guidelines in selecting the suitable setup.

3.2.1 *Single emission region and external seed photons*

The first point that we consider is the possibility that the two peaks of the SED are produced by a single emitting region (hence by the same electron population) but with target photons for the IC scattering being provided by an external region (without this last condition we would fall in the SSC model previously excluded). In the structured jet scenario the emission region could be the layer and the external radiation is that produced by the spine, or *viceversa*. Indeed this was the original set-up discussed in Ghisellini et al. (2005), in which the entire SED of radio–galaxies was attributed to the layer.

This possibility is disfavored for the case of NGC 1275 (as for the previous case of M87 in TG08) because it requires a Doppler factor not compatible with the inferred relatively large viewing angle $\theta_{\rm v} \gtrsim 20^\circ$. Briefly, the reasoning leading to this conclusion develops through the following three steps : i) the frequency of the IC peak, $\nu_{\rm IC}$, provides a lower limit for the Lorentz factor of the electrons emitting at the peaks of the SED, $\gamma_{\rm p}$; ii) this limit, coupled to the observed synchrotron peak frequency $\nu_{\rm s}$, provides an upper limit for the ratio of the magnetic field and the Doppler factor B/δ; iii) the observed high energy flux limits the level of the SSC component: the magnetic field cannot be smaller than a critical value. This, coupled with the B/δ upper limit derived above, constrains δ to be larger than a critical value, that can be achieved only for small angles, no matter the value of Γ.

More quantitatively the steps are the following:

- If the IC peak is produced in the KN regime, the energy of the electrons at the peak are comparable to the photons energies, i.e. $\gamma_{\rm p} m_{\rm e} c^2 \delta \simeq h\nu_{\rm IC}$. If, on the other hand, the peak is produced in the Thomson regime, the peak frequency would be $\nu_{\rm IC} \simeq \gamma_{\rm p}^2 \nu'_{\rm ext} \delta$ (where $\nu'_{\rm ext}$ is the peak frequency of the external radiation field in the comoving frame of the emitting source) with the Thomson

condition $\gamma_{\rm p} h\nu'_{\rm ext} < m_{\rm e}c^2$, which provides $\gamma_{\rm p} m_{\rm e}c^2\delta > h\nu_{\rm IC}$. Inserting the numerical values, the Lorentz factor of the electrons emitting at the peak would therefore be $\gamma_{\rm p} \gtrsim 8\times10^3\delta^{-1}\nu_{\rm IC,24}$.

- The observed synchrotron peak frequency $\nu_{\rm s} \simeq 2.8\times10^6 B\gamma_{\rm p}^2\,\delta$ Hz with the limit derived above for $\gamma_{\rm p}$ implies $B/\delta < 0.056\,\nu_{\rm s,13}\,\nu_{\rm IC,24}^{-2}$ G.
- With the value of $\gamma_{\rm p}$ and $\nu_{\rm s}$, the SSC component is predicted to peak at a frequency $\nu_{\rm SSC}\simeq 10^{21}/\delta^2$ Hz. Its luminosity therefore is limited by the observed hard X-ray flux. Looking at the SED we can write this condition as:

$$\frac{L_{\rm SSC}}{L_{\rm s}} = \frac{U'_{\rm s}}{U_B} \lesssim 0.1 \;\rightarrow\; \frac{L_{\rm s}}{4\pi R^2 c\, U_B \delta^4} \lesssim 0.1. \qquad (2)$$

Using the limit on B derived above and expressing the radius as $R < ct_{\rm var}\delta$ we find:

$$\delta \gtrsim 3.5\, L_{\rm s,43.5}^{1/8}\,\nu_{\rm IC,24}^{1/2}\,\nu_{\rm s,13}^{-1/4} t_{\rm var,1w}^{-1/4}, \qquad (3)$$

in which we have assumed the (conservative) value $t_{\rm var} = 1$ week.

Note that the case $\gamma_{\rm p} = h\nu_{\rm IC}/m_{\rm e}c^2\delta$ — corresponding to scattering in the Thomson–KN transition — is the most conservative one in terms Doppler factor. In fact, larger values of $\gamma_{\rm p}$ imply smaller magnetic fields and thus larger Doppler factors to keep the SSC luminosity below the limit. We remark that the above inference only assumes that the seed photons for scattering are not synchrotron. Therefore the conclusion is valid not only for a structured jet, but also when the external radiation originates in the environment surrounding the jet (e.g. from accretion or dust).

The derived lower limit for the Doppler factor, although not extreme, requires $\theta_{\rm v} \lesssim 16.5^\circ$, smaller than the value $\theta_{\rm v} \gtrsim 20^\circ$ estimated by radio observations (see A14). Moreover the situation is even more complex due to the fact that for $\theta_{\rm v}\sim 10^\circ$ and Lorentz factors $\Gamma_{\rm s}\sim 10$, $\Gamma_{\rm l}\sim 3$–4, the Doppler factors of both components are very similar, making unlikely that a single component dominates the entire SED. For smaller still angles, the emission from the spine starts to dominate the SED. In Fig. 1 (top panel) we report our fit for $\theta_{\rm v} = 6^\circ$, implying that NGC 1275 is a blazar. The dashed red and the thin solid blue line show the contribution of the spine and the layer to the total emission, clearly dominated by the spine. The high-energy bump is a mix of SSC (in the X–ray band) and IC off the photons of the layer (the peak in the γ–ray band). The corresponding parameters are reported in the first raw of Tab. 1.

Although the model reproduces quite satisfactorily the SED, the implied angle is clearly not consistent with the values derived from radio observations. Given this difficulty, the possibility of a single emitting region seems rather unlikely. In the next section we therefore consider the case with a large $\theta_{\rm v}$ and with both regions contributing to the emission.

3.2.2 Two–component model

After the discussion in the previous section we are left with two alternative possibilities: either the spine produces the observed synchrotron component and the layer the high–energy component or, conversely, the spine produces the γ–ray emission and the layer the low frequency peak.

In the latter case, the spine would produce a SED strongly unbalanced toward the IC peak, since the synchrotron luminosity must be low enough not to contribute to the observed emission, $L_{\rm IC} \gg L_{\rm s}$. In this case, the corresponding emission from the spine as seen by an observer aligned with the jet would be even more extreme, since the ratio between the IC (by construction mainly produced by the scattering of the photons from the layer) and the synchrotron luminosities increases for smaller angles (Dermer 1995, TG08). The resulting source would appear as a strongly IC dominated BL Lac object, for which there are no representatives in current samples of blazars.

The most plausible solution is thus to associate the low–energy component with the synchrotron emission of the spine and the high–energy bump to the IC emission of the layer. This is the solution we discuss in the following.

In Fig. 1 (second and third panels) we report the results of our model for two different viewing angles, $\theta_{\rm v} = 18^\circ$ and 25°. As discussed above, we suppose that the spine (red line) is responsible for the low energy bump, while the high-energy component is the result of the layer IC component (blue). To produce γ–rays, the electrons of the layer have quite large Lorentz factors, $\gamma_{\rm max}\sim 10^6$. The corresponding synchrotron frequency falls in the X–ray band. To not overproduce the flux in this band we keep a low value of the layer magnetic field. Clearly, the emission from the layer is strongly unbalanced in favor of the IC emission, dominated by the scattering off the IR photons of the spine. When setting the parameters of the spine we are guided by the requirements to produce a SED dominated by the synchrotron component. However, we also require that the IC component is not too low. This requirement follows from the fact that, once observed at smaller angles, one expects to observe a SED similar to that of typical low synchrotron peaked BL Lac objects (see below). In this case it is likely that the IC component, peaking in the soft γ–ray band, substantially contributes to the observed X–ray continuum. Note that, due to the low luminosity and the relatively high frequency of the synchrotron peak of the layer, the resulting contribution of this radiation field to the IC emission from the spine is negligible (thus the IC peak is dominated by the SSC component). In analogy with the case of M87, we adopt bulk Lorentz factors $\Gamma_{\rm s} = 10$ and $\Gamma_{\rm l} = 4$. The relative Lorentz factor is $\Gamma_{\rm rel} = 1.46$. The value of the spine is typically derived for BL Lac objects (e.g. Ghisellini et al. 2010), sources for which the spine should dominate the entire SED. In the case of the layer, we adopt a value similar to that used for M87. Having fixed these parameters we try to find the set of the remaining parameters that better reproduce the data.

For $\theta_{\rm v} = 18^\circ$ the model can satisfactorily reproduce the observed high–energy bump. For $\theta_{\rm v} = 25^\circ$, however, the model fails in reproducing the data at the highest energies. The reason for this problem, already discussed in TG08 for the case of M87 but more severe here, is the huge photon–photon absorption of the high-energy γ–rays produced in the layer by the dense IR–optical radiation field of the spine. While for the case $\theta_{\rm v} = 18^\circ$ the intrinsic (i.e. beaming corrected) synchrotron luminosity of the spine is still low enough to make the source transparent for photons at few hundreds of GeV, for $\theta_{\rm v} = 25^\circ$ the optical depth exceeds unity above few tens of GeV, causing an abrupt cut–off of the emission. The optical depth can be approximated by (e.g. Dondi & Ghisellini 1995):

$$\tau_{\gamma\gamma}(E) \simeq \frac{\sigma_{\rm T}}{5} r\, n'(\epsilon')\epsilon' \qquad (4)$$

where r is the jet radius and $n'(\epsilon')\epsilon'$ is the soft photons number density in the layer frame, calculated at the threshold energy $\epsilon' = m^2c^4\delta/E$:

$$n'(\epsilon')\epsilon' \simeq \frac{\epsilon' L'_s(\epsilon')}{4\pi r^2 c\,\epsilon'} = \frac{\epsilon L_s(\epsilon)\Gamma_{\rm rel}^2}{4\pi r^2 c\,\epsilon'\delta_{\rm s}^4} \qquad (5)$$

	R cm	H cm	$L_{\rm syn}$ erg s^{-1}	B G	$\gamma_{\rm min}$	$\gamma_{\rm b}$	$\gamma_{\rm max}$	n_1	n_2	Γ	$\theta_{\rm v}$ deg.
Layer	5×10^{16}	2×10^{16}	10^{40}	0.3	150	10^4	2×10^5	1	3.3	3	6
Spine	5×10^{16}	10^{15}	2×10^{40}	0.08	60	1.9×10^3	5×10^4	1.9	3.5	10	6
Layer	5×10^{16}	2×10^{16}	6.5×10^{40}	0.9	150	150	10^6	1	2.5	4	18
Spine	5×10^{16}	10^{15}	1.3×10^{43}	2.5	60	8×10^2	1.5×10^4	2.3	2.5	10	18
Layer	5×10^{16}	2×10^{16}	5×10^{41}	2	600	100	5×10^6	1	2.5	4	25
Spine	5×10^{16}	10^{15}	1.5×10^{44}	8.5	5	5	1.5×10^4	1	2.5	10	25

Table 1. Input parameters of the models for the layer and the spine shown in Fig. 1. All quantities (except the bulk Lorentz factors Γ and the viewing angle $\theta_{\rm v}$) are measured in the rest frame of the emitting plasma. The external radius of the layer is fixed to the value $R_2 = 1.2\times R$.

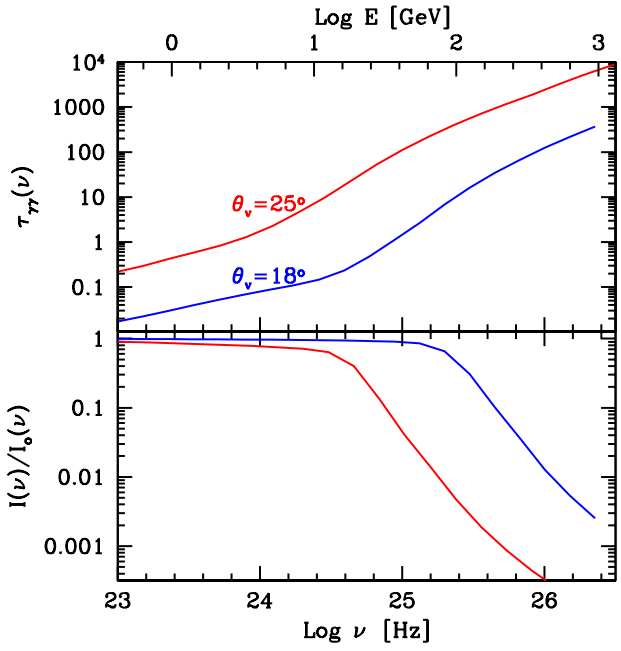

Figure 2. Optical depth (upper panel) and suppression factor (lower panel) for absorption of γ–rays within the jet as a function of the frequency for the two models reported in Fig. 1, for $\theta_{\rm v} = 18^{\rm o}$ (blue) and $\theta_{\rm v} = 25^{\rm o}$ (red).

where $\delta_{\rm s}^4$ is used to transform the observed synchrotron luminosity to the spine rest frame and $\Gamma_{\rm rel}^2$ is the boosting term of the photon energy density from the spine to the layer frame. For a fixed observed luminosity of the target photons, the optical depth depends strongly on the Doppler factor, as $\delta_{\rm s}^{-4}$. In Fig. 2, we show the optical depth and the corresponding "suppression factor" $[1-\exp(-\tau_{\gamma\gamma})]/\tau_{\gamma\gamma}$ as a function of the frequency, in the two cases. The shape of the curves, which reflects the spectrum of the target photons, is similar in both cases, but the case $\theta_{\rm v} = 25^{\rm o}$ implies an optical depth larger by a factor of ≈ 10, as expected from the ratio of the two boosting factors in the two cases, $(1.86/1.02)^4 \sim 11$. For $\theta_{\rm v} = 18^{\rm o}$ the source is transparent ($\tau_{\gamma\gamma} < 1$) up to ~ 100 GeV. Instead, for $\theta_{\rm v} = 25^{\rm o}$, the optical depth reaches unity already at 20–30 GeV and rapidly increases, determining the abrupt cut–off visible in Fig. 1 (lower panel).

An effect possibly mitigating the importance of the opacity, not treated in our calculations, is related to the anisotropy of the soft photon target field. In fact, in the frame of the layer, the γ–ray photons eventually reaching us make an angle of $\sim 90^{\circ}$ with the jet axis, while the target photons, produced by the spine, are going along the jet axis. The γ–rays and their targets therefore preferentially collide with an angle of 90°.

Since the threshold condition for the reaction depends on the angle, $\epsilon' E' = 2m^2c^4/(1-\cos\theta)$, this translates into a shift to higher ν by a factor ≈ 2 of the curves in Fig. 2. This, coupled to the presence of another factor $(1-\cos\theta)$ in the expression of the optical depth, implies an effective decrease of τ at a given frequency. However, while the effect could be important for frequencies for which $\tau \sim 1$ (i.e. around $\nu = 10^{24}$ Hz for the case $\theta_{\rm v}$=25°), its impact on the suppression factor at larger frequencies, for which the optical depth rapidly reaches $\tau \gg 1$, is almost negligible.

Focusing on the case for $\theta_{\rm v} = 18^{\rm o}$, the power carried by the jet (assuming a composition of one cold proton per emitting electron, e.g. Celotti & Ghisellini 2008) is $P_{\rm j,l} = 6\times10^{43}$ erg s^{-1} and $P_{\rm j,s} = 2.3\times10^{47}$ erg s^{-1} for the layer and the spine, respectively. The corresponding radiative luminosities (corrected for beaming) are $L_{\rm r,l} = 2\times10^{43}$ erg s^{-1} and $L_{\rm r,s} = 2\times10^{45}$ erg s^{-1}. The coupling with the spine radiation field makes the layer extremely efficient to convert kinetic power into radiation, with an efficiency $\eta_{r,l} = P_{\rm j,l}/L_{\rm r,l} \simeq 30\%$. The spine power appears quite large, more similar to the average power inferred for the powerful flat spectrum radio quasar than those of BL Lac objects (e.g., Ghisellini et al. 2010). The mass of the black hole in NGC 1275 is estimated to be around $M_{\rm BH} \sim 3\times10^8 M_{\odot}$ (Woo & Urry 2002), corresponding to an Eddington luminosity of $L_{\rm Edd} \approx 4.2\times10^{46}$ erg s^{-1}. The jet power is thus about a factor of 5 larger, consistent with what generally inferred by studies of the jet of blazars (e.g. Ghisellini et al. 2010).

Fig. 3 shows the SED calculated for the case $\theta_{\rm v} = 18^{\circ}$ as would be recorded by an observer located at $\theta_{\rm v} = 6^{\circ}$ from the jet axis (solid black line). This SED would thus correspond to that of the blazar associated to the misaligned jet of NGC 1275 (numerical values of the flux correspond to the blazar located at the same redshift as NGC 1275). The synchrotron peak located in the optical band would lead to classify the source as a BL Lac object with the peak in the IR band. The overall shape of the SED observed at $\theta_{\rm v} = 6^{\circ}$ resembles (apart from the γ–ray emission) the shape of the BL Lac object 1420+5422 ($z = 0.153$, Shaw et al. 2013), which is however a factor $\sim$15 less luminous than the "aligned" NGC 1275. In fact the data of 1420+5422 (green data points, from `http://tools.asdc.asi.it`) have been increased by a factor 15.

Finally we discuss the possible role of an environmental radiation field. In fact, any soft ambient radiation field, beamed in the layer frame, could contribute to the IC emission. Unfortunately the knowledge of the nuclear environment of NGC 1275 is far from complete. As for the other FRI radio galaxies, the lack of broad

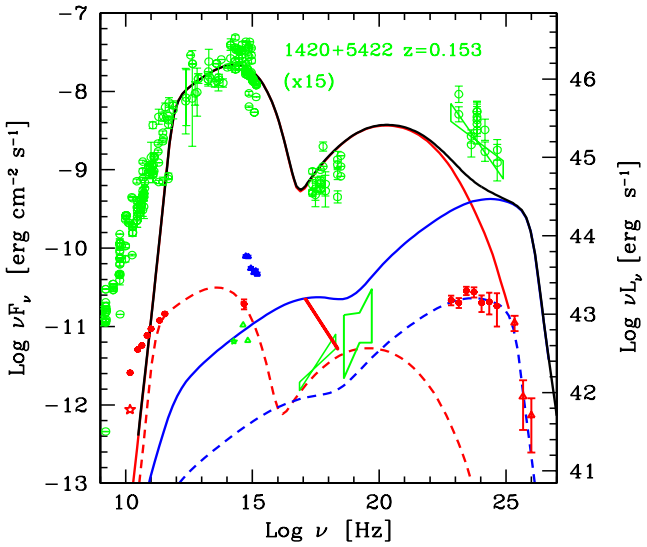

Figure 3. The black line shows the emission from the spine-layer model of NGC 1275 for the case $\theta_{\rm v} = 18^\circ$ (left panel in Fig. 1 and dashed red and blue lines) as observed at $\theta_{\rm v} = 6^\circ$. The solid red and blue lines shows the separate contribution of the spine and the layer, respectively. For comparison, the green data points (associated to the luminosity, right y-axis) describe the SED of 1420+5422, a BL Lac at $z = 0.153$ with a luminosity multiplied by a factor of 15 (data from `http://tools.asdc.asi.it`).

emission lines leads to the idea that any accretion flow should be quite inefficient. We can derive a robust upper limit on the luminosity of the nuclear component from the measured IR flux of the core (green star in Fig. 1), likely associated to the non–thermal emission from the inner regions of the jet (Baldi et al. 2010), $L_{\rm env} < 3 \times 10^{42}$ erg s^{-1}. The contribution of the external radiation is maximized if its emission occurs within a region with size of the order of the distance of the emission region in the jet, d. Larger sizes would lead to the dilution of the energy density (proportional to $1/d^2$), while for lower distances the radiation field in the jet frame would be deebosted. Assuming a jet aperture angle ψ, the distance of the emission region is $d \sim r/\psi$, and the ratio of the external energy density to the spine energy density in the frame of the layer can be estimated to be:

$$\frac{U'_{\rm env}}{U'_{\rm s}} < \frac{L_{\rm env}}{L_{\rm s}} \left(\frac{\Gamma_{\rm l}}{\Gamma_{\rm rel}}\right)^2 \psi^2 \delta_{\rm s}^4. \qquad (6)$$

Inserting the numerical values (assuming $\psi = 0.1$) we find that $U'_{\rm env}/U'_{\rm s} < 0.1$ and thus any possible radiation field can be safely neglected. Besides being a source of target photons for the IC process, an external radiation field could also act as an absorber for the γ–rays produced by the jet. For an external radiation field with a narrow spectrum peaking at an energy $\epsilon_{\rm ext} = h\nu_{\rm ext} = 0.4\,\nu_{\rm ext,14}$ eV, the maximum of the optical depth would correspond to an energy $E = m^2c^4/\epsilon_{\rm ext} = 0.6\,\nu_{\rm ext,14}^{-1}$ TeV, i.e close to the MAGIC points at the highest energies. A simple estimate of the optical depth at this energy yields $\tau_{\gamma\gamma} \lesssim 2/d_{18}$ (assuming a distance $d \approx 10^{18}$ cm). This upper limit to the optical depth due to the environment is then smaller than the internal absorption.

4 DISCUSSION

Summarizing, we have shown that the overall SED of NGC 1275 can be satisfactorily reproduced in the framework of the "spine-layer" model — with bulk Lorentz factors for the two components similar to those used in the case of M87 — if the viewing angle is smaller then $\theta_{\rm v} \sim 20$ deg. Larger angles inevitably lead to a drastic suppression of the emission in the MAGIC energy band caused by the strong internal absorption of the γ–rays with energies above few tens of GeV, determined by the luminous IR radiation field associated to the spine emission.

Estimates of the angle at pc scale, based on the detection of the counter jet, provide values in the range 30–55 degrees (Walker et al. 1994, Asada et al. 2006). However, smaller angles are often assumed (e.g. Abdo et al. 2009). A much lower value ($\theta_{\rm v} \approx 3^\circ$) at sub–pc scale was derived from VLBI observations by Krichbaum et al. (1992). Considering these uncertainties and the not unlikely possibility that the jet bends from the sub–pc scale (where we suppose that the emission occurs) to the pc scales imaged with VLBI, we conclude that the spine–layer scenario is clearly constrained but still barely suitable to reproduce the data. A strong test able to seriously threaten the model would be the detection of photons at energies above 1 TeV, for which, even with $\theta_{\rm v} = 18^\circ$, the optical depth $\tau_{\gamma\gamma} > 10^3$, corresponding to a suppression of the flux exceeding 10^3.

A point not completely satisfactory about our preferred model for $\theta_{\rm v} = 18^\circ$ concerns the emission the jet would present if observed at smaller angles. As previously discussed in TG08, in the unification scheme for radio–galaxies and blazars we generally expect that, once observed at small angles, the non–thermal continuum from a radiogalaxy resembles that of a blazar. In particular, for NGC 1275 we expect that the SED shape follows that of high–power BL Lac objects. We indeed found a source whose SED shape closely traces our theoretical curve, but with a luminosity about one order of magnitude smaller than the beamed emission of NGC 1275.

A14 report the existence of a clear correlation between the LAT γ–ray flux, F_γ, and the optical flux, $F_{\rm opt}$, compatible with both a linear ($F_\gamma \propto F_{\rm opt}$) and a quadratic ($F_\gamma \propto F_{\rm opt}^2$) dependence. In our scheme the flux in the two bands is dominated by the emission produced in two separate regions, i.e. the spine for the optical and the layer for the γ–rays. In principle several possibilities are allowed by this configuration. For instance, γ–ray variability without counterpart in the optical is possible with changes of the parameters of the layer (in particular those specifying the electron energy distribution) and a stationary spine emission. On the other hand, since the IC emission of the layer — responsible for the observed high–energy emission — is dominated by the scattering of the synchrotron photons of the spine, we expect that variations of the optical emission are accompanied by variations in the γ–ray band. If such variations are driven by changes in the intrinsic emissivity of the spine, without changes in the structural parameters (in particular the bulk Lorentz factor) we expect a linear correlation. However, if variations of $\Gamma_{\rm s}$ (and/or of $\Gamma_{\rm l}$) are also involved, more complex patterns are possible, connected to the interplay between the beaming of the emission in the observer frame and the amplification of the energy density of the seed photons, depending on the relative motion of the spine and the layer. With such a complex phenomenology is difficult to clearly identify a mechanism for the observed correlation. The simplest situation, corresponding to a linear correlation, is associated to variations of the electron energy distribution or of the magnetic field of the spine.

ACKNOWLEDGMENTS

We thank the referee for the insightful and constructive comments that helped us to greatly improve the paper. FT acknowledges contribution from a grant PRIN–INAF–2011. Part of this work is based on archival data, software or on-line services provided by the ASI Science Data Center.

REFERENCES

Abdo A. A., et al., 2009, ApJ, 699, 31
Ajello M., et al., 2009, ApJ, 690, 367
Aharonian F., et al., 2006, Sci, 314, 1424
Aharonian F., et al., 2009, ApJ, 695, L40
Aleksić J., et al., 2012, A&A, 539, L2
Aleksić J., et al., 2014, A&A, 564, A5
Asada K., Kameno S., Shen Z.-Q., Horiuchi S., Gabuzda D. C., Inoue M., 2006, PASJ, 58, 261
Baldi R. D., et al., 2010, ApJ, 725, 2426
Balmaverde B., Capetti A., Grandi P., 2006, A&A, 451, 35
Brown A. M., Adams J., 2011, MNRAS, 413, 2785
Celotti A., Ghisellini G., 2008, MNRAS, 385, 283
Chiaberge M., Capetti A., Celotti A., 1999, A&A, 349, 77
Chiaberge M., Celotti A., Capetti A., Ghisellini G., 2000, A&A, 358, 104
Dondi L., Ghisellini G., 1995, MNRAS, 273, 583
Fabian A. C., et al., 2011, MNRAS, 418, 2154
Georganopoulos M., Kazanas D., 2003, ApJ, 594, L27
Ghisellini G., Celotti A., Fossati G., Maraschi L., Comastri A., 1998, MNRAS, 301, 451
Ghisellini G., Tavecchio F., Chiaberge M., 2005, A&A, 432, 401
Ghisellini G., Tavecchio F., Foschini L., Ghirlanda G., Maraschi L., Celotti A., 2010, MNRAS, 402, 497
Giroletti M., Giovannini G., Cotton W. D., Taylor G. B., Pérez-Torres M. A., Chiaberge M., Edwards P. G., 2008, A&A, 488, 905
Kataoka J., et al., 2010, ApJ, 715, 554
Krichbaum T. P., et al., 1992, A&A, 260, 33
Nagai H., et al., 2010, PASJ, 62, L11
Nagai H., et al., 2014, ApJ, 785, 53
Shaw M.S., et al., 2013, ApJ, 764, 135
Tavecchio F., Ghisellini G., 2008, MNRAS, 385, L98
Walker R. C., Romney J. D., Benson J. M., 1994, ApJ, 430, L45
Woo J.-H., Urry C. M., 2002, ApJ, 579, 530